Letter | Editors' Suggestion

Observation of gapped Dirac magnons in a Co bilayer grown on Ru(0001)

Khalil Zakeri [1,*] Arthur Ernst [2,3,4] and Christopher Hins [1]

[1]*Heisenberg Spin-dynamics Group, Physikalisches Institut, Karlsruhe Institute of Technology, Wolfgang-Gaede-Strasse 1, D-76131 Karlsruhe, Germany*

[2]*Institute for Theoretical Physics, Johannes Kepler University, Altenberger Strasse 69, A-4040 Linz, Austria*

[3]*Max-Planck-Institut für Mikrostrukturphysik, Weinberg 2, D-06120 Halle (Saale), Germany*

[4]*Donostia International Physics Center, Donostia-San Sebastian, 20018 Gipuzkoa, Spain*

(Received 23 February 2026; revised 1 October 2026; accepted 9 October 2026; published 27 October 2026)

Beyond their fundamental interest in exploring bosonic Dirac physics, Dirac magnons hold potential for the development of efficient spin-transport devices. Here, we demonstrate the experimental realization of gapped terahertz Dirac magnons in an epitaxial Co bilayer on Ru(0001) using spin-polarized electron spectroscopy. Supported by first-principles calculations, we show that although the substrate breaks sublattice symmetry, thereby opening a gap at the $\bar{K}$ points, the local valley topology is preserved. This is evidenced by a spectral weight redistribution, valley-centered curvature concentrations, and a nonzero local Berry phase. Our results establish the interface as a tuning parameter, paving the way for engineering Dirac magnons in a variety of simple ultrathin bilayer magnets.

DOI: 10.1103/cprf-rwsn

The discovery of topological phases of matter has fundamentally reshaped our understanding of condensed-matter systems, extending well beyond the fermionic realm of electrons in graphene and topological materials to bosonic excitations [1–8]. Among these, Dirac magnons, characterized by symmetry-protected features, have emerged as a frontier in quantum magnetism [8–22]. Fundamentally, these massless quasiparticles offer a unique framework to explore the interplay between lattice symmetry, sublattice interactions, and the topology of the magnonic bands [23–25].

From an application perspective, these symmetry-protected magnons offer a compelling platform for next-generation spintronics and magnonics, providing viable routes toward efficient spin transport and highly tunable magnon Hall effects, both of which prevent the Joule heating inherent to conventional electronic currents. Notably, Dirac magnons operating at the terahertz (THz) scale are intrinsically resilient against thermal noise, enabling robust room-temperature operation. Beyond transport, they may provide a playground for testing topological bosonic quantum phenomena that are otherwise obscured by thermal noise in conventional low-energy bosonic systems.

Despite this profound potential, the experimental realization and manipulation of THz Dirac magnons remain challenging. A central challenge lies in identifying simple material systems where such magnons are accessible to spectroscopic probes and are easily tunable [13,14].

Symmetry arguments establish that a bilayer hexagonal-close-packed (hcp) ferromagnet is host to Dirac magnons at the $\bar{K}$ point of the surface Brillouin zone (SBZ). The underlying physics of these topological excitations is fundamentally analogous to Dirac fermions in graphene, where the sublattice symmetry enforces a linear crossing of the dispersion relations [3,26]. In this case, the layer index of the bilayer serves as a pseudospin degree of freedom, mathematically isomorphic to the A and B sublattices of a honeycomb lattice [8,14,16,17,26,27]. Consequently, the interlayer exchange coupling acts as the magnonic counterpart to the electronic hopping parameter, mediating the interaction strength across the magnetic lattice. This structural equivalence ensures that the magnon Hamiltonian, when linearized near the $\bar{K}$ point, takes the form of the Dirac equation, giving rise to magnonic Dirac cones [26,28,29]. This correspondence permits the description of magnons as massless bosons, with a group velocity fundamentally governed by the strength of the exchange interactions [see Supplemental Material (SM) Note I [30]].

Very recently, this prediction has been expanded to a broad class of layered structures characterized by C_{3v} symmetry, reflecting a major push toward high-throughput material discovery in topological magnonics [31,32].

An important consideration is that in realistic device architectures, magnetic films are grown on substrates that impose lattice mismatch strain, symmetry breaking, and most importantly, proximity effects. These interfacial phenomena can significantly modify the system's intrinsic magnetic properties. Consequently, several critical questions arise: (i) Can the magnonic Dirac cone be realized experimentally in a realistic hcp ferromagnetic bilayer? (ii) How does the substrate environment dictate the stability and the local topological character, specifically the local Berry curvature and Berry phase, of these excitations? (iii) Would these ultrathin magnetic films on a metallic substrate possess a nonzero Berry phase?

*Contact author: khalil.zakeri@partner.kit.edu

Published by the American Physical Society under the terms of the Creative Commons Attribution 4.0 International license. Further distribution of this work must maintain attribution to the author(s) and the published article's title, journal citation, and DOI.

In this Letter, we address these open questions by investigating a prototypical system: an hcp Co bilayer epitaxially grown on a Ru(0001) substrate. We provide direct experimental evidence for the existence of Dirac magnons at the high-symmetry $\bar{K}$ point of the SBZ. Crucially, despite the influence of the substrate, the resulting magnonic states retain their local topological character and nonzero Berry phase. Our results demonstrate that the substrate not only lifts the degeneracy of the magnonic Dirac point but also redistributes the Berry curvature over a broader region of momentum space. This extended curvature can drive an anomalous velocity [33] over a large fraction of momentum space, offering compelling prospects for THz magnon (spin) transport. Consequently, we establish that the substrate serves not merely as a passive support, but as an active tuning parameter. Finally, we propose a systematic route to restore the Dirac point and the quantized Berry phase via a magnetic symmetrization of the system.

Magnetic excitations were investigated using spin-polarized high-resolution electron energy-loss spectroscopy (SPHREELS), a technique uniquely suited for probing magnons in ultrathin magnetic structures across the entire SBZ [34–37]. In SPHREELS, a monochromatic, spin-polarized electron beam excites the magnons and the subsequently scattered electrons carry the fundamental characteristics of these excitations, including their energy (frequency), wave vector (wavelength), and lifetime [38–41]. All experiments were conducted at room temperature. The scattering geometry is schematically illustrated in the inset of Fig. 1, with the scattering plane aligned along the $\bar{\Gamma}$-$\bar{K}$-$\bar{M}$ symmetry path of the SBZ. The spin-polarization vector $\boldsymbol{P}$ was oriented either parallel or antiparallel to the scattering plane's normal vector $\hat{\boldsymbol{n}}$. The energy distribution of the scattered electrons was recorded for both orientations of $\boldsymbol{P}$, yielding two partial intensity spectra, $I_\uparrow$ and $I_\downarrow$. As shown in Fig. 1, these spectra exhibit signatures of both spin-dependent (magnons) and spin-independent (vibration) excitations [42]. The difference $I_{\text{diff}} = I_\downarrow - I_\uparrow$ [or asymmetry $A = (I_\downarrow - I_\uparrow)/(I_\downarrow + I_\uparrow)$] spectra effectively isolate the magnetic excitations, allowing the dispersion to be mapped across the entire SBZ through a series of constant-momentum scans (see SM Note II [30]).

The experimental intensity map of I_{diff}, probed across the energy-momentum space along the $\bar{\Gamma}$-$\bar{K}$-$\bar{M}$ high-symmetry path of the SBZ, is presented in Fig. 2. Near the zone center ($\bar{\Gamma}$ point) and in the midway of $\bar{\Gamma}$-$\bar{K}$, the spectra are dominated by a prominent acoustic magnon mode characterized by a notably stiff dispersion relation. As the momentum increases toward the $\bar{K}$ point, a secondary optical mode becomes more pronounced at higher energies, exhibiting a comparatively soft dispersion. At the $\bar{K}$ point, these two modes converge to form a gapped Dirac crossing, a hallmark of the broken inversion symmetry in this bilayer system. To elucidate the physical origin of the observed intensity profile and confirm the protected nature of the crossing, we compared the experimental data with results derived from *ab initio* calculations. To ensure that all experimental features were accurately captured, we employed a theoretical framework combining first-principles calculations with atomistic linear spin-wave theory. Our approach incorporates three critical factors that extend beyond

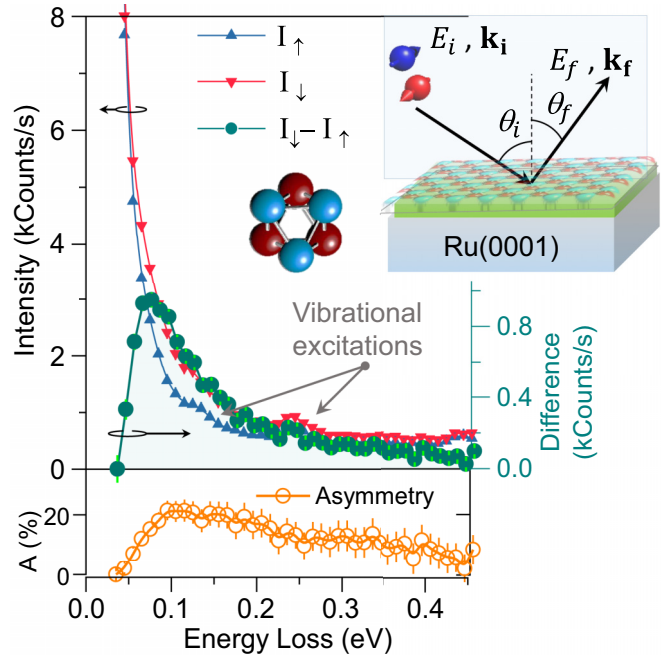


FIG. 1. SPHREEL spectra. The spectra were recorded at a wave vector of $q = -0.7$ Å^{-1}, using an incident energy of $E_i = 4$ eV. The partial intensity spectra are denoted by $I_\uparrow$ ($I_\downarrow$), where the subscripts $\uparrow$ ($\downarrow$) represent the direction of the spin polarization vector $\boldsymbol{P}$, being parallel (antiparallel) to the magnetization $\boldsymbol{M}$, respectively. The asymmetry $A = (I_\downarrow - I_\uparrow)/(I_\downarrow + I_\uparrow)$ plot is shown in the lower panel. The data clearly resolve the presence of both the first (acoustic) mode at an energy of approximately 70 meV and the second (optical) mode centered around 330 meV. The difference spectrum represents the magnon signal. A schematic representation of the scattering geometry is provided in the inset. The atomic structure of the hcp bilayer is also depicted, where the first and second layers are distinguished by dark red and dark blue spheres, respectively.

simplified models: (i) noninteger, layer-dependent magnetic moments; (ii) long-range exchange couplings J_{ij} extending significantly beyond the first coordination shell; and (iii) the intrinsic surface sensitivity of the experimental technique. Following the determination of these magnonic parameters, we calculated the magnonic band structure and the Bloch spectral function. The final intensity map was then simulated by incorporating the surface sensitivity profile inherent to the SPHREELS probe, which primarily samples the outermost layer of the film (see SM Note II [30]). This approach facilitates a more direct comparison between the predicted spectral weight and the experimental observations. For a direct comparison, the resulting calculated intensity map is presented alongside the experimental data in Fig. 2, with the calculated magnon dispersion branches superimposed on both maps as solid curves. These calculations assume pseudomorphic growth of the Co film, where the in-plane lattice parameter is constrained to the Ru(0001) substrate ($a_\parallel = 2.706$ Å), while the interlayer spacing is allowed to relax to its experimental value [43,44]. To isolate the effects of epitaxial strain, we also present the magnon dispersion for a hypothetical unstrained scenario in which the system adopts the bulk Co in-plane lattice parameter ($a_\parallel = 2.506$ Å, dashed curves). The differ-

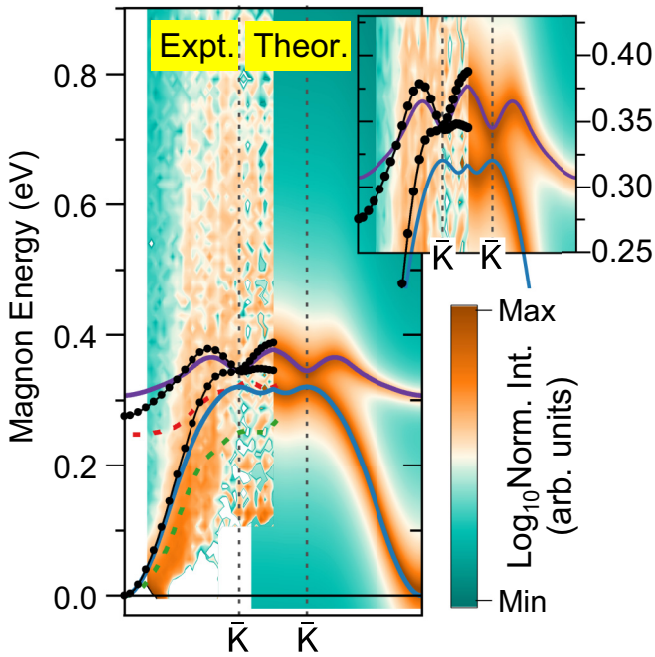


FIG. 2. Intensity map of magnetic excitations in energy–momentum space. The logarithmic-scale map is plotted along the high-symmetry $\bar{\Gamma}$-$\bar{K}$-$\bar{M}$ direction (excluding the $\bar{M}$ point). Experimental results are presented on the left, with corresponding theoretical calculations on the right. A magnified view near the Dirac crossing is provided in the upper-right-hand corner, highlighting the intensity inversion between the acoustic and optical branches across the crossing point. Solid and dashed curves indicate the calculated dispersion relations for relaxed structures using the in-plane lattice parameters of Ru(0001) and Co(0001), respectively. Black circles represent the calculations with symmetrized exchange parameters (see text). A schematic representation of the SBZ is provided in Fig. S1 [30].

ence in spectral broadening between theory and experiment is primarily due to the system's itinerant character. Specifically, the persistence of the experimental intensity up to 0.8 eV is driven by intrinsic lifetime broadening and incoherent single-particle background contributions. Furthermore, the suppressed optical magnon intensity near the zone center is consistent with the dynamic structure factor and selection rules, while the low-energy intensity near the zone-boundary $\bar{K}$ point arises from a broadened quasielastic tail under extreme kinematic conditions and residual surface adsorbates (see also SM Note II [30]). Despite the notable damping of these modes, our results confirm the presence of gapped Dirac magnons at the $\bar{K}$ point. This topological feature is experimentally manifested by a striking intensity inversion (or "flipping") between the acoustic and optical branches in the immediate vicinity of the $\bar{K}$ point. This redistribution of spectral weight, where the maximum intensity shifts from one branch to the other upon crossing the high-symmetry point, serves as the signature of a Dirac crossing. This behavior is fundamentally analogous to the pseudospin character switching observed in the Dirac fermions of graphene, where the wave-function character is transferred between the two sublattices across the Dirac point [3]. In magnonic systems, this intensity flip provides a direct experimental visualization of the rapid rotation of the magnon wave functions, a mechanism that constitutes the physical origin of the nonzero Berry phase. This is further supported by a self-consistent framework of three experimental observations: (i) dispersion dynamics, i.e., the convergence of magnonic branches, (ii) spectral weight redistribution and constant-energy slices consistent with a gapped Dirac crossing and a nonzero Berry phase, and (iii) the robustness of these features against inherent Landau damping (see SM Note III [30]).

It is important to note that the gap at the Dirac crossing is an extrinsic effect arising from the substrate. In a freestanding hcp Co bilayer, the two layers are equivalent, and the Dirac point is protected by this layer (sublattice) symmetry. This symmetry guarantees a twofold degeneracy corresponding to the two-dimensional irreducible representation E of the C_{3v} magnetic point group, as discussed in Ref. [31]. In the present case, the Ru(0001) substrate breaks the sublattice symmetry, as evidenced by the distinct intralayer exchange parameters of the interface layer ($J_{1\parallel}^{\mathrm{Int.}} \approx 6.1$ meV) and the surface layer ($J_{1\parallel}^{\mathrm{Surf.}} \approx 10.8$ meV), along with their respective magnetic moments $\mu^{\mathrm{Int.}} \approx 1.34\mu_B$, $\mu^{\mathrm{Surf.}} \approx 1.65\mu_B$ (see Fig. S2 [30] for a comprehensive comparison). This imbalance acts as an effective staggered potential that lifts the Dirac degeneracy, opening a 25 meV gap between the lower branch (peaking at 320 meV) and the upper branch (with a minimum at 345 meV). To confirm this, calculations performed with artificially symmetrized parameters ($J_{i,j\parallel}^{\mathrm{Int.}} = J_{i,j\parallel}^{\mathrm{Surf.}}$ and $\mu^{\mathrm{Int.}} = \mu^{\mathrm{Surf.}}$) are presented as solid circles in Fig. 2. These results demonstrate the restoration of the Dirac point at the $\bar{K}$ point. In this symmetric limit, the magnon bands carry a Berry phase of π (see SM Note IV [30]). Note that the effective coupling in the magnon Hamiltonian scales as $J_{ij}/\sqrt{\mu_i \mu_j}$ (see SM Note II [30]). Consequently, the reduction in J_{ij} values observed in the interface layer is partially compensated by the simultaneous decrease in the magnetic moments μ_i of this layer. This correlation is a characteristic feature of itinerant magnetism, where both exchange interactions and magnetic moments are self-consistently determined by the electronic structure. To quantify the local topological properties, we mapped the Berry curvature $\Omega_n(\omega, \boldsymbol{q})$, with the results presented in Fig. 3 (see also the animation provided in SM [30]). Note that since the Berry phase and Berry curvature are geometric properties and not direct physical observables, their identification relies on detecting their measurable consequences, i.e., an intensity winding about the Dirac crossing. In Fig. 3(a), Ω is encoded on the magnonic band structure. As is clearly seen, the 25 meV gap serves as a focal point for the system's topology. The band-resolved 2D maps of $\Omega_n(\boldsymbol{q})$ presented in Figs. 3(b) and 3(c), for the upper and lower bands, respectively. The results reveal that the $\Omega_n(\omega, \boldsymbol{q})$ is somewhat localized near the gapped Dirac points in the form of Berry flux poles. It seems that despite the physical gap, the magnonic wave functions undergo a rapid rotation in the pseudospin space near the high-symmetry $\bar{K}$ points, making these regions act as intense sources (or sinks) of a fictitious magnetic field. Integrating the $\Omega_n(\boldsymbol{q})$ along a loop of radius 0.37 Å^{-1} (half of the $\bar{M}$-$\bar{K}$ path) around $\bar{K}$ yields a Berry phase of $\approx 0.3\pi$. This nonquantized value confirms that the substrate-induced gap broadens

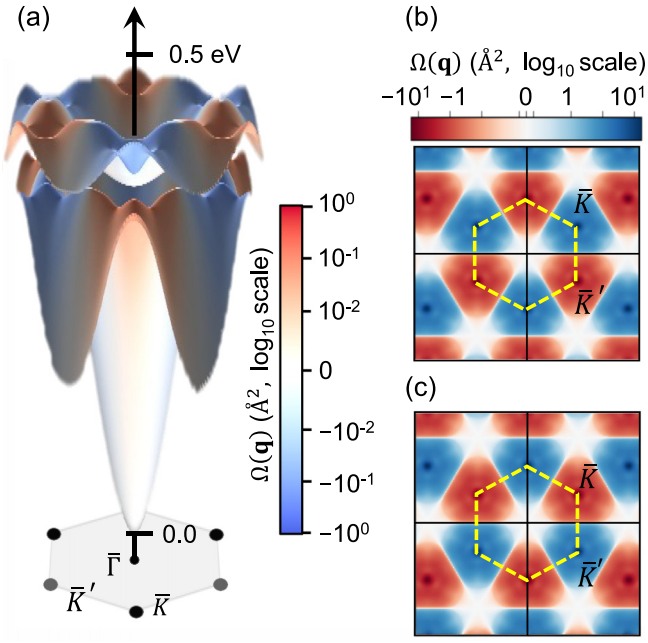


FIG. 3. Calculated energy-momentum mapping of the Berry curvature. (a) Visualization of the Berry curvature for an hcp Co bilayer on Ru(0001), projected onto the magnon bands. The color scale represents the Berry curvature Ω. (b), (c) 2D Berry curvature maps for the top and bottom bands, respectively. All color bars use a symmetric logarithmic scale. The results reveal intense poles at the high-symmetry $\bar{K}$ and $\bar{K}'$ points. While the substrate breaks inversion symmetry and lifts the Dirac degeneracy, the localized Berry curvature demonstrates that the bands retain their intrinsic topological character. See the animation in SM [30].

the Berry flux, which is no longer singular. This leads to a radius dependence of the Berry phase (see SM Note V [30]). Critically, the Berry curvature is perfectly antisymmetric between valleys, $\Omega_n(\bar{K}) = -\Omega_n(\bar{K}')$, a condition enforced by the mirror symmetry of the bilayer. While this antisymmetry ensures a vanishing total Chern number ($C = 0$) and renders a net anomalous magnon Hall effect symmetry forbidden, the effect remains accessible through the selective excitation of individual magnon populations. Importantly, these enlarged poles remain a robust fingerprint of the gapped Dirac physics, acting as a "symmetry-protected topological memory" that dictates the intrinsic dynamics of these high-energy magnons.

It should be emphasized that our primary objective is not merely to quantify the magnitude of the gap itself. Rather, our central finding is that magnons at the high-symmetry $\bar{K}$ point carry a nonzero local Berry phase even in the presence of such a substrate-induced gap.

The observed Dirac-like crossing and the associated Berry curvature redistribution serve as the essential parent phase for a magnonic topological insulator. This system can be driven into a topologically nontrivial state with a nonzero Chern number by introducing interfacial Dzyaloshinskii-Moriya interactions [45–47].

The magnonic band gap at the $\bar{K}$ point can be tuned, and the quantized Berry phase restored, through a "magnetic symmetrization" of the heterostructure. This can be achieved by depositing a few atomic layers of Ru as a capping layer, which equalizes the chemical environment at both interfaces and effectively restores the sublattice interchange symmetry [31]. Furthermore, our calculations demonstrate that alternative symmetrization approaches, such as adding a Pd monolayer, can substantially reduce the potential gradient between the sublattices, thereby facilitating the emergence of a Dirac point at $\bar{K}$ (see SM Note VI [30]). Beyond restoring the requisite magnetic symmetry, the inclusion of Pd can effectively suppresses Landau damping [30,40].

In conclusion, we have provided direct experimental evidence for the existence of gapped Dirac magnons in an epitaxial hcp Co bilayer on Ru(0001). Using SPHREELS, we probed the magnonic spectrum over a large fraction of the SBZ and identified the intensity flipping of the magnon spectral weight in the vicinity of the $\bar{K}$ points, an observation fundamentally related to the rapid rotation of the magnonic wave functions in pseudospin space. While broad spectral features are an inherent physical property of itinerant magnets, the identification of a Dirac crossing is supported by a self-consistent framework comprising several experimental observations: (i) dispersion dynamics, (ii) spectral weight redistribution, (iii) constant-energy slices, and (iv) intensity winding around the crossing point. Our findings demonstrate that while the Ru(0001) substrate breaks sublattice symmetry and opens a finite gap at the $\bar{K}$ points, the underlying local valley topology and the local nonzero Berry curvature remain intact, characterized by intense Berry curvature poles distributed over a broader region of momentum space. Our work establishes that the substrate is not merely a passive support but may be regarded as a tuning parameter for engineering local topological features in ultrathin magnetic films. The Dirac point and its associated quantized Berry phase can, in principle, be recovered through the magnetic symmetrization of the layers. The results can be extended to various hcp ferromagnetic bilayers far beyond the investigated system [48,49]. In principle, one can consider the inclusion of antisymmetric exchange interactions or extend these findings to hcp and triangular magnetic insulators in the form of ultrathin slabs [45,47,50–52]. Beyond providing a potential playground for bosonic Dirac physics, these findings pave the way for a new generation of magnonic devices and the realization of tunable topological thermal Hall effects in layered and nanostructured quantum magnets [53].

Financial support by the Deutsche Forschungsgemeinschaft (DFG) through the DFG Grants No. ZA 902/8-1 and No. ZA 902/9-1. A.E. acknowledges the funding by the Fonds zur Förderung der wissenschaftlichen Forschung (FWF) under Grant No. I 5384. K.Z. thanks the Physikalisches Institut for hosting the group and providing the necessary infrastructure.

Data availability. The data that support the findings of this article are openly available [73].

[1] F. D. M. Haldane, Model for a quantum Hall effect without landau levels: Condensed-matter realization of the "parity anomaly", Phys. Rev. Lett. **61**, 2015 (1988).

[2] C. L. Kane and E. J. Mele, Z_2 topological order and the quantum spin Hall effect, Phys. Rev. Lett. **95**, 146802 (2005).

[3] A. H. Castro Neto, F. Guinea, N. M. R. Peres, K. S. Novoselov, and A. K. Geim, The electronic properties of graphene, Rev. Mod. Phys. **81**, 109 (2009).

[4] M. Z. Hasan and C. L. Kane, *Colloquium*: Topological insulators, Rev. Mod. Phys. **82**, 3045 (2010).

[5] L. Lu, J. D. Joannopoulos, and M. Soljačić, Topological photonics, Nat. Photonics **8**, 821 (2014).

[6] Y. Liu, Y. Xu, and W. Duan, Berry phase and topological effects of phonons, Natl. Sci. Rev. **5**, 314 (2018).

[7] T. Ozawa, H. M. Price, A. Amo, N. Goldman, M. Hafezi, L. Lu, M. C. Rechtsman, D. Schuster, J. Simon, O. Zilberberg, and I. Carusotto, Topological photonics, Rev. Mod. Phys. **91**, 015006 (2019).

[8] J. Fransson, A. M. Black-Schaffer, and A. V. Balatsky, Magnon Dirac materials, Phys. Rev. B **94**, 075401 (2016).

[9] A. Mook, J. Henk, and I. Mertig, Tunable magnon Weyl points in ferromagnetic pyrochlores, Phys. Rev. Lett. **117**, 157204 (2016).

[10] S. A. Owerre, Dirac magnon nodal loops in quasi-2D quantum magnets, Sci. Rep. **7**, 6931 (2017).

[11] S. Bao, J. Wang, W. Wang, Z. Cai, S. Li, Z. Ma, D. Wang, K. Ran, Z.-Y. Dong, D. L. Abernathy, S.-L. Yu, X. Wan, J.-X. Li, and J. Wen, Discovery of coexisting Dirac and triply degenerate magnons in a three-dimensional antiferromagnet, Nat. Commun. **9**, 2591 (2018).

[12] W. Yao, C. Li, L. Wang, S. Xue, Y. Dan, K. Iida, K. Kamazawa, K. Li, C. Fang, and Y. Li, Topological spin excitations in a three-dimensional antiferromagnet, Nat. Phys. **14**, 1011 (2018).

[13] L. Chen, J.-H. Chung, B. Gao, T. Chen, M. B. Stone, A. I. Kolesnikov, Q. Huang, and P. Dai, Topological spin excitations in honeycomb ferromagnet CrI_3, Phys. Rev. X **8**, 041028 (2018).

[14] B. Yuan, I. Khait, G.-J. Shu, F. C. Chou, M. B. Stone, J. P. Clancy, A. Paramekanti, and Y.-J. Kim, Dirac magnons in a honeycomb lattice quantum XY magnet $CoTiO_3$, Phys. Rev. X **10**, 011062 (2020).

[15] M. Elliot, P. A. McClarty, D. Prabhakaran, R. D. Johnson, H. C. Walker, P. Manuel, and R. Coldea, Order-by-disorder from bond-dependent exchange and intensity signature of nodal quasiparticles in a honeycomb cobaltate, Nat. Commun. **12**, 3936 (2021).

[16] L. Chen, M. B. Stone, A. I. Kolesnikov, B. Winn, W. Shon, P. Dai, and J.-H. Chung, Massless Dirac magnons in the two dimensional van der Waals honeycomb magnet $CrCl_3$, 2D Mater. **9**, 015006 (2022).

[17] J. A. Schneeloch, Y. Tao, Y. Cheng, L. Daemen, G. Xu, Q. Zhang, and D. Louca, Gapless dirac magnons in $CrCl_3$, npj Quantum Mater. **7**, 66 (2022).

[18] S.-H. Do, K. Kaneko, R. Kajimoto, K. Kamazawa, M. B. Stone, J. Y. Y. Lin, S. Itoh, T. Masuda, G. D. Samolyuk, E. Dagotto, W. R. Meier, B. C. Sales, H. Miao, and A. D. Christianson, Damped Dirac magnon in the metallic kagome antiferromagnet FeSn, Phys. Rev. B **105**, L180403 (2022).

[19] S. E. Nikitin, B. Fåk, K. W. Krämer, T. Fennell, B. Normand, A. M. Läuchli, and C. Rüegg, Thermal evolution of Dirac magnons in the honeycomb ferromagnet $CrBr_3$, Phys. Rev. Lett. **129**, 127201 (2022).

[20] P. A. McClarty, Topological magnons: A review, Annu. Rev. Condens. Matter Phys. **13**, 171 (2022).

[21] M. dos Santos Dias, N. Biniskos, F. J. dos Santos, K. Schmalzl, J. Persson, F. Bourdarot, N. Marzari, S. Blügel, T. Brückel, and S. Lounis, Topological magnons driven by the Dzyaloshinskii-Moriya interaction in the centrosymmetric ferromagnet Mn_5Ge_3, Nat. Commun. **14**, 7321 (2023).

[22] X. Chen, Y. Liu, P. Liu, Y. Yu, J. Ren, J. Li, A. Zhang, and Q. Liu, Unconventional magnons in collinear magnets dictated by spin space groups, Nature (London) **640**, 349 (2025).

[23] K. Zakeri, Probing of the interfacial Heisenberg and Dzyaloshinskii–Moriya exchange interaction by magnon spectroscopy, J. Phys.: Condens. Matter **29**, 013001 (2017).

[24] K. Zakeri, Terahertz magnonics: Feasibility of using terahertz magnons for information processing, Physica C **549**, 164 (2018).

[25] K. Zakeri, Magnonic crystals: Towards terahertz frequencies, J. Phys.: Condens. Matter **32**, 363001 (2020).

[26] S. S. Pershoguba, S. Banerjee, J. C. Lashley, J. Park, H. Ågren, G. Aeppli, and A. V. Balatsky, Dirac magnons in honeycomb ferromagnets, Phys. Rev. X **8**, 011010 (2018).

[27] A. Scheie, P. Laurell, P. A. McClarty, G. E. Granroth, M. B. Stone, R. Moessner, and S. E. Nagler, Dirac magnons, nodal lines, and nodal plane in elemental gadolinium, Phys. Rev. Lett. **128**, 097201 (2022).

[28] X. S. Wang and X. R. Wang, Topological magnonics, J. Appl. Phys. **129**, 151101 (2021).

[29] H. Walker, Topological magnetism turns elementary, Physics **15**, 30 (2022).

[30] See Supplemental Material at http://link.aps.org/supplemental/10.1103/cprf-rwsn for (i) a simple model demonstrating the emergence of Dirac magnons with symmetry-protected properties in hcp bilayers, (ii) specific details regarding our experimental and theoretical methodologies, (iii) further evidence for the Dirac character and the nonzero Berry phase of magnons in the investigated system, (iv) the magnonic properties of the artificially symmetrized Co bilayer on Ru, (v) the radius dependence of the Berry phase, (vi) restoring the Dirac point via magnetic symmetrization, and (vii) an animation showing the Berry curvature mapped onto the magnonic band structure from multiple perspectives, which includes Refs. [54–72].

[31] K. Zakeri and A. Ernst, Dimensionality-driven terahertz Dirac magnons in layered 3*d* ferromagnets, Nano Lett. **26**, 2660 (2026).

[32] K. Zakeri, C. Hins, R. R. Neumann, A. Mook, and A. Ernst, Dirac magnons in a thin elemental itinerant ferromagnet, Sci. Adv. **12**, eaed9835 (2026).

[33] R. Matsumoto and S. Murakami, Theoretical prediction of a rotating magnon wave packet in ferromagnets, Phys. Rev. Lett. **106**, 197202 (2011).

[34] J. Prokop, W. X. Tang, Y. Zhang, I. Tudosa, T. R. F. Peixoto, K. Zakeri, and J. Kirschner, Magnons in a ferromagnetic monolayer, Phys. Rev. Lett. **102**, 177206 (2009).

[35] K. Zakeri and J. Kirschner, Probing magnons by spin-polarized electrons, in *Magnonics*, edited by S. Demokritov and A. Slavin, Topics in Applied Physics (Springer, Berlin, 2013), Vol. 125, Chap. 7, pp. 84–99.

[36] K. Zakeri, Elementary spin excitations in ultrathin itinerant magnets, Phys. Rep. **545**, 47 (2014).
[37] K. Zakeri and C. Berthod, Theory of spin-polarized high-resolution electron energy loss spectroscopy from nonmagnetic surfaces with a large spin-orbit coupling, Phys. Rev. B **106**, 235117 (2022).
[38] Y. Zhang, T.-H. Chuang, K. Zakeri, and J. Kirschner, Relaxation time of terahertz magnons excited at ferromagnetic surfaces, Phys. Rev. Lett. **109**, 087203 (2012).
[39] K. Zakeri, Y. Zhang, T.-H. Chuang, and J. Kirschner, Magnon lifetimes on the Fe(110) surface: The role of spin-orbit coupling, Phys. Rev. Lett. **108**, 197205 (2012).
[40] H. J. Qin, K. Zakeri, A. Ernst, L. M. Sandratskii, P. Buczek, A. Marmodoro, T. H. Chuang, Y. Zhang, and J. Kirschner, Long-living terahertz magnons in ultrathin metallic ferromagnets, Nat. Commun. **6**, 6126 (2015).
[41] K. Zakeri, A. Hjelt, I. V. Maznichenko, P. Buczek, and A. Ernst, Nonlinear decay of quantum confined magnons in itinerant ferromagnets, Phys. Rev. Lett. **126**, 177203 (2021).
[42] Y. Zhang, P. A. Ignatiev, J. Prokop, I. Tudosa, T. R. F. Peixoto, W. X. Tang, Kh. Zakeri, V. S. Stepanyuk, and J. Kirschner, Elementary excitations at magnetic surfaces and their spin dependence, Phys. Rev. Lett. **106**, 127201 (2011).
[43] F. El Gabaly, S. Gallego, C. Muñoz, L. Szunyogh, P. Weinberger, C. Klein, A. K. Schmid, K. F. McCarty, and J. de la Figuera, Imaging spin-reorientation transitions in consecutive atomic Co layers on Ru(0001), Phys. Rev. Lett. **96**, 147202 (2006).
[44] F. E. Gabaly, J. M. Puerta, C. Klein, A. Saa, A. K. Schmid, K. F. McCarty, J. I. Cerda, and J. de la Figuera, Structure and morphology of ultrathin Co/Ru(0001) films, New J. Phys. **9**, 80 (2007).
[45] K. Zakeri, Y. Zhang, J. Prokop, T.-H. Chuang, N. Sakr, W. X. Tang, and J. Kirschner, Asymmetric spin-wave dispersion on Fe(110): Direct evidence of the Dzyaloshinskii-Moriya interaction, Phys. Rev. Lett. **104**, 137203 (2010).
[46] K. Zakeri, A. Marmodoro, A. von Faber, S. Mankovsky, and H. Ebert, Chirality-inverted Dzyaloshinskii-Moriya interaction, Phys. Rev. B **108**, L100403 (2023).
[47] K. Zakeri, A. von Faber, S. Mankovsky, and H. Ebert, Unraveling the complexity of the Dzyaloshinskii–Moriya interaction in layered magnets: The full magnitude and chirality control, Adv. Mater. **37**, 2500152 (2025).
[48] K. Zakeri, H. Qin, and A. Ernst, Unconventional magnonic surface and interface states in layered ferromagnets, Commun. Phys. **4**, 18 (2021).
[49] K. Zakeri, A. von Faber, and A. Ernst, Magnons and fundamental magnetic interactions in a ferromagnetic monolayer: The case of the Ni monolayer, Phys. Rev. B **109**, L180406 (2024).
[50] K. Zakeri, Y. Zhang, J. Prokop, T. H. Chuang, W. X. Tang, and J. Kirschner, Magnon excitations in ultrathin Fe layers: The influence of the Dzyaloshinskii-Moriya interaction, J. Phys.: Conf. Ser. **303**, 012004 (2011).
[51] S. Tsurkan and K. Zakeri, Giant Dzyaloshinskii-Moriya interaction in epitaxial Co/Fe bilayers with C_{2v} symmetry, Phys. Rev. B **102**, 060406(R) (2020).
[52] K. Zakeri and A. von Faber, Giant spin-orbit induced magnon nonreciprocity in ultrathin ferromagnets, Phys. Rev. Lett. **132**, 126702 (2024).
[53] K. Zakeri and A. Ernst, Generation and propagation of ultrafast terahertz magnons in atomically architectured nanomagnets, Nano Lett. **24**, 9528 (2024).
[54] K. Zakeri, T. Peixoto, Y. Zhang, J. Prokop, and J. Kirschner, On the preparation of clean tungsten single crystals, Surf. Sci. **604**, L1 (2010).
[55] R. Vollmer, M. Etzkorn, P. S. Anil Kumar, H. Ibach, and J. Kirschner, Spin-polarized electron energy loss spectroscopy of high energy, large wave vector spin waves in ultrathin fcc Co films on Cu(001), Phys. Rev. Lett. **91**, 147201 (2003).
[56] M. Etzkorn, P. S. Anil Kumar, W. Tang, Y. Zhang, and J. Kirschner, High-wave-vector spin waves in ultrathin Co films on W(110), Phys. Rev. B **72**, 184420 (2005).
[57] M. Etzkorn, P. S. Anil Kumar, R. Vollmer, H. Ibach, and J. Kirschner, Spin waves in ultrathin Co-films measured by spin polarized electron energy loss spectroscopy, Surf. Sci. **566-568**, 241 (2004).
[58] M. Etzkorn, P. S. A. Kumar, and J. Kirschner, High- energy Surface spin waves studied by spin-polarized electron energy loss spectroscopy, *Handbook of Magnetism and Advanced Magnetic Materials* (Wiley, Hoboken, NJ, 2007), pp. 1658–1684.
[59] K. Zakeri, D. Rau, J. Wettstein, M. Döttling, J. Jandke, F. Yang, W. Wulfhekel, and J. Schmalian, Direct evidence of a charge depletion region at the interface of van der Waals monolayers and dielectric oxides: The case of superconducting FeSe/STO, Phys. Rev. B **107**, 184508 (2023).
[60] J. Kirschner, Direct and exchange contributions in inelastic scattering of spin-polarized electrons from iron, Phys. Rev. Lett. **55**, 973 (1985).
[61] J. P. Perdew, K. Burke, and M. Ernzerhof, Generalized gradient approximation made simple, Phys. Rev. Lett. **77**, 3865 (1996).
[62] L. Szunyogh, B. Újfalussy, P. Weinberger, and J. Kollár, Self-consistent localized KKR scheme for surfaces and interfaces, Phys. Rev. B **49**, 2721 (1994).
[63] A. I. Liechtenstein, M. I. Katsnelson, V. P. Antropov, and V. A. Gubanov, Local spin density functional approach to the theory of exchange interactions in ferromagnetic metals and alloys, J. Magn. Magn. Mater. **67**, 65 (1987).
[64] Y.-J. Chen, K. Zakeri, A. Ernst, H. J. Qin, Y. Meng, and J. Kirschner, Group velocity engineering of confined ultrafast magnons, Phys. Rev. Lett. **119**, 267201 (2017).
[65] S. Paischer, D. Eilmsteiner, I. Maznichenko, N. Buczek, K. Zakeri, A. Ernst, and P. A. Buczek, Correlations, disorder, and multimagnon processes in terahertz spin dynamics of magnetic nanostructures: A first-principles investigation, Phys. Rev. B **109**, L220405 (2024).
[66] D. Xiao, M.-C. Chang, and Q. Niu, Berry phase effects on electronic properties, Rev. Mod. Phys. **82**, 1959 (2010).
[67] T. Fukui, Y. Hatsugai, and H. Suzuki, Chern numbers in discretized Brillouin zone: Efficient method of computing (spin) Hall conductances, J. Phys. Soc. Jpn. **74**, 1674 (2005).
[68] L. F. Zhang, J. Ren, J. S. Wang, and B. W. Li, Topological magnon insulator in insulating ferromagnet, Phys. Rev. B **87**, 144101 (2013).
[69] T. Skovhus and T. Olsen, Dynamic transverse magnetic susceptibility in the projector augmented-wave method: Application to Fe, Ni, and Co, Phys. Rev. B **103**, 245110 (2021).
[70] K. Zakeri, T.-H. Chuang, A. Ernst, L. Sandratskii, P. Buczek, H. Qin, Y. Zhang, and J. Kirschner, Direct probing of the

exchange interaction at buried interfaces, Nat. Nanotechnol. **8**, 853 (2013).

[71] K. Zakeri, Y. Zhang, and J. Kirschner, Surface magnons probed by spin-polarized electron energy loss spectroscopy, J. Electron Spectrosc. Relat. Phenom. **189**, 157 (2013).

[72] P. Buczek, A. Ernst, and L. M. Sandratskii, Different dimensionality trends in the Landau damping of magnons in iron, cobalt, and nickel: Time-dependent density functional study, Phys. Rev. B **84**, 174418 (2011).

[73] K. Zakeri, A. Ernst, and C. Hins, Data of 2 ML Co on Ru(0001), Zenodo, 2026, https://doi.org/10.5281/zenodo.18742712.